ISSN 2682-681X (Paper), ISSN 2705-4241 (Online) | http://unilorinjoger.com | https://doi.org/10.63745/joger.2025.12.30.006

JOURNAL OF GEOMATICS AND ENVIRONMENTAL RESEARCH
www.unilorinjoger.com

RESEARCH ARTICLE

Spatio-Temporal Monitoring of Subsea Infrastructure Displacement, Seabed Morphodynamics, and Flow Velocity Variability

Hart, Lawrence, Jackson, K.P., Clifford Oribikunomaa

Department of Surveying and Geomatics
Rivers State University, Port Harcourt, Nigeria

Corresponding email: lawrence.hart@ust.edu.ng

Abstract

Subsea infrastructure in tidal rivers is highly vulnerable due to dynamic sedimentary processes intensified by dredging, sand mining, and vessel traffic, creating a high-risk corridor for pipelines and flowlines. The New Calabar River in the Niger Delta illustrates these hazards, where active morphodynamics threaten pipeline integrity and elevate the risk of environmental contamination. This study applied a positivist, quantitative framework to conduct multi-epoch monitoring of seabed evolution and its implications for pipeline stability. GNSS positioning supported spatial control, a sub-bottom profiler was used to assess infrastructure displacement, and a current meter provided flow velocity data across a 1.5 km² survey area. Results show pronounced morphological instability, with burial depth varying from 3.00 m to 0.30 m. Erosion and accretion volumes were 1,627,031.61 m³ and 1,010,959.09 m³, respectively, indicating a significant sediment imbalance. The pipeline experienced a 2–3 m southward shift driven by tidal currents and channel migration. Average flow velocity was 0.532 m/s, peaking at 0.798 m/s. These findings identify zones where reduced burial depth increases the risk of exposure to hydrodynamic forces and navigational impacts. The study demonstrates the value of geomatics-based assessments for enhancing the resilience of subsea energy infrastructure, supporting SDG 7 and mitigating ecological risks aligned with SDGs 14 and 15.

ARTICLE HISTORY
Received: 9th October, 2025
Accepted: 26th November, 2025
Published: 5th December, 2025

KEYWORDS
Subsea Infrastructure
Tidal River
Sediment Transport
GNSS
SDGs

Citation: Hart Lawrence, Jackson K.P, Clifford Oribikunomaa (2025). Spatio-Temporal Monitoring of Subsea Infrastructure Displacement, Seabed Morphodynamics, and Flow Velocity Variability, *Journal of Geomatics and Environmental Research, 8(2). Pp56-68*

1. INTRODUCTION

Subsea infrastructure is fundamental to the transport of oil and gas and supports critical sectors such as energy, dredging, and telecommunications. In fluvial and estuarine systems like the New Calabar River, these installations are typically buried beneath the riverbed to shield them from mechanical damage, environmental stressors, and sediment mobility. Burial depth, therefore, governs the resilience of pipelines and flowlines against tidal forces, hydrodynamic currents, and long-term sediment transport processes (Zhang et al., 2023; Leckie et al., 2018).

However, the stability of subsea infrastructure in tidal rivers is increasingly compromised by dynamic sedimentary processes. In the New Calabar River, strong tidal currents mobilize large sediment loads, driving erosion, accretion, and channel migration. These processes alter pipeline alignment, reduce burial depth, and jeopardize structural integrity (Cheng et al., 2014; Leckie *et al*., 2018). Pipelines conveying crude oil and gas face heightened risk, as exposure increases susceptibility to scour, free-spanning, and mechanical damage. Anthropogenic pressures, including intensified vessel traffic, further elevate the likelihood of anchor strikes on exposed or shallow-buried infrastructure. Insufficient burial-depth updates

and weak anchorage regulations exacerbate vulnerabilities, particularly where vortex-induced vibrations or anchor dragging may occur (Wu, Yang & Sun, 2025).

The river's morphology is shaped by tidal forcing, variable river discharge, and human activities such as dredging, spoil disposal, and hydrocarbon development. These drivers modify sediment pathways, influence burial conditions, and expose pipelines to scour, subsidence, and lateral displacement. As a tidal waterway linked to the Atlantic Ocean, the New Calabar River experiences complex interactions between saline tidal inflows and freshwater discharge, producing dynamic hydro-sedimentary regimes that regulate deposition and erosion (Ibe & Awosika, 1991; Eze *et al*., 2021). Prior research highlights the rapid and often unpredictable sedimentation patterns in Niger Delta Rivers, underscoring persistent risks to buried infrastructure (Ibe & Awosika, 1991; Ajdehak et al., 2018). Consequently, understanding sediment structure interactions is essential for evaluating pipeline vulnerability, supporting geospatial monitoring, and informing sustainable marine resource management.

This study investigates subsea infrastructure stability along a section of the New Calabar River. The specific objectives are to: (i) assess the positional shift of existing subsea infrastructure using geospatial techniques; (ii) quantify erosion and accretion volumes within the study area; and (iii) determine the flow velocity regime influencing seabed morphodynamics.

2. STUDY AREA

The study area is located within projected coordinates 275528.54 mE 506669.71 mN, 277688.09mE, 506781.35mN, 277743.09mE, 506029.03mN, and 275513.32mE, 505906.91mN. The section of study is 3km in length and 0.55km in width, as illustrated in Plate 1. The New Calabar River forms part of the broader Niger Delta region, which is characterized by diverse ecological and geophysical features. The dynamic sedimentary environment, combined with dredging, sand mining, and vessel traffic, creates a high-risk corridor for subsea infrastructure such as pipelines and flowlines. The New Calabar River, located within Nigeria's maritime domain, exhibits a highly dynamic sedimentary regime that poses significant challenges to subsea infrastructure stability. Its seabed comprises heterogeneous materials—ranging from fine silts and clays to coarse sands and organic deposits, which respond differently to burial, erosion, and compaction processes.

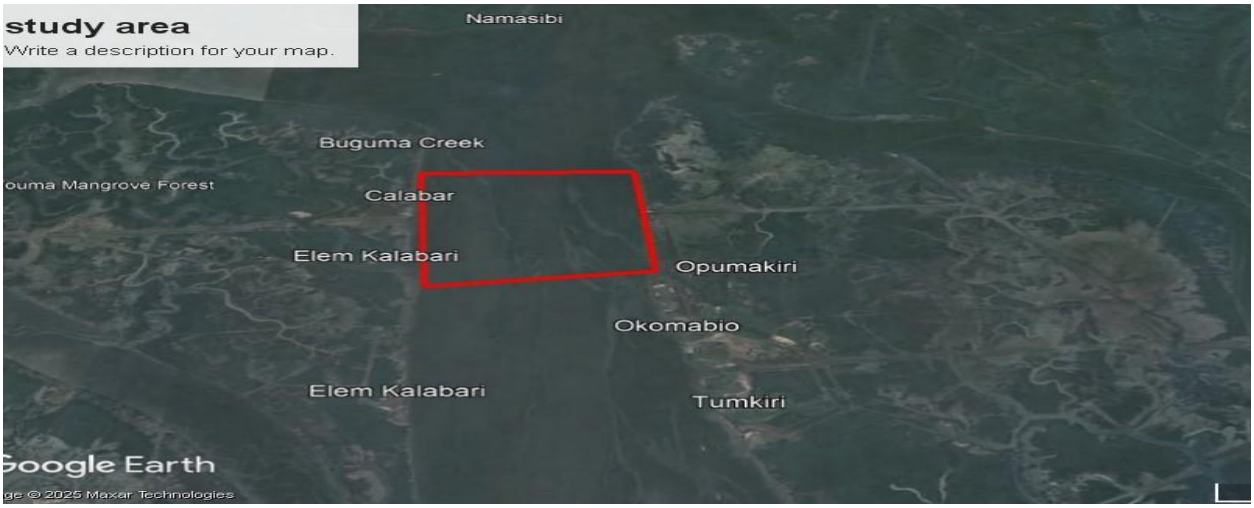

Plate 1: Map Showing New Calabar River
(Source: Google Earth 2024)

3. METHODOLOGY

3.1 Materials and Methods

The methods employed for data acquisition in this study are essential for accurately determining the seabed and subsurface features. According to Oye et al. (2021), GNSS is utilized for surface positioning, employing the trilateration method to determine positions on the Earth or near-earth surfaces. The process adopted the Differential Global Positioning System (DGPS), which is capable of detecting errors such as satellite clock drift, orbital perturbations, and atmospheric delays affecting microwave transmission, which are modelled to give improved derived positional values.

Moreover, the acoustic system of seabed interrogation relies on sound pulses propagating through water. By transmitting a pulse and recording the two-way travel time, depth or subsurface features can be determined accurately, as outlined by Basil (2024). The equipment utilized in this study includes a DGPS receiver (C-Nav 3050), Meridian Gyro compass, Motion Sensor (TSS Motion Sensor), Leveling staff, Sub-bottom Profiling EdgeTech 3100 (SB216S), Side Scan Sonar (StarFish 990F), Magnetometer (Geometric G882), Valeport CM106 current meter, and MV DATLOG as the survey boat.

Furthermore, the software utilized for data analysis includes Hypack MagLog Lite, Seanet Pro, Notepad, Microsoft Excel/Word, SonarWiz, Surfer, Vale Port Datalog X2 software, ArcGIS/QGIS, and AutoCAD software. These software tools assist in processing and interpreting the collected data for further analysis and mapping, as described by Orupabo (2002).

The combined use of various methods and tools for data acquisition in this study ensures accurate positioning and detection of seabed and subsurface features, as it affects the seabed infrastructure in the study area. The integration of GNSS, acoustic systems, and magnetic variation monitoring enhances the overall efficiency and reliability of the data collected for further analysis and interpretation.

The Hypack, Integrated Navigation Software, was used to aid data acquisition. This software is designed to accept raw data, such as data from the DGPS receiver and bearing from the gyro. It displays a visual representation of the real-time orientation and position of the dynamic object on its helmsman display. Once the appropriate input layback and offset (see Table 1) of the primary sensor offsets parameters on the vessel objects (sensors deployed during the study, such as SSS, Sub-bottom Profiler, and magnetometer tow-fishes, and Echo-sounder transducer) are made, the software computes their corresponding positions. The software can serve as a digital storage device for all position data, the logged bathymetry, and various sensors' data. It can also be used to transmit position data to other equipment. During the setting-up phase, the instrument offset position referenced to the CRP is made. With the various deployed instrument offsets (listed in Table 1), the corresponding positions are computed by the Hypack software from the DGPS receiver. Layback (a function of the vessel CRP (Common Reference Point) and located on the Along Axis (y)) can be computed using a modified form of Pythagoras' Theorem.

Table1. Sensor Offsets Parameters on the Hydrographic Vessel

	Athwart X (m)	Along Y (m)
CRP (Mid-Stern)	0.00	0.00
Motion Sensor	0.00	3.00
DGPS	-1.10	2.60
Echo Sounder	-1.10	1.50
Sub-Bottom Profiler	1.10	1.50
Side Scan Sonar	-1.10	2.00
Magnetometer	1.10	0.40

(**Source: NCI 2024)**

3.2 Flow Measurement with Current Meter Valeport CM 106

The Valeport CM 106 is a propeller-type current meter that was operated in a self-recording and logging mode as well as direct reading (real-time) mode. To have a reliable measurement with Valeport CM 106, the inner part of the impeller was filled with water, and the meter was balanced in a horizontal position before being launched into the water. The suspension assembly was moved along the main frame to quickly achieve balance. Sub-bottom Profiling EdgeTech 3100 (SB216S) to detect pipeline burial and positional changes, Side Scan Sonar (StarFish 990F) for acoustic riverbed imaging, Magnetometer (Geometric G882 Cesium Magnetometer) for environmental magnetic variation monitoring, Valeport CM106 current meter for flow measurements, and an MV DATLOG as the survey boat.

The Manning equation is an empirical formula widely used in hydraulics and hydrology to estimate the average flow velocity of water in open channels (e.g., rivers, canals, drainage systems). It helps in the estimation of discharge capacity, sediment transport potential, and flood risks in natural rivers. It is also useful in analyzing flow velocity in tidal rivers, which directly influences sediment mobility and potential pipeline exposure.

It is expressed as:

$$V = \frac{1}{n} R^{2/3} S^{1/2} \quad (1.0)$$

Where V is the mean flow velocity, n = Manning's roughness coefficient (dimensionless), representing channel resistance (depends on bed material, vegetation, obstructions), and S is the Channel slope (energy grade line or bed slope, it is dimensionless)

$$R = Hydraulic\ Radius(m) = \frac{A}{P} \quad (2.0)$$

Volume Computation Analysis

The volume computation using a model means using a structured mathematical approach to determine how much material exists between surfaces or boundaries. The accuracy depends on the quality of the model, so in this study surface differencing model was used to compare the two surfaces of deposition and erosion. To represent the erosion and deposition of different grain sizes and the development of an armored surface layer, an active layer system is used. When material is added to the top active layer, material is removed from this layer and added to the next layer down, as in equation 3.0.

$$E_1 = \left(\frac{F_i^x}{\sum F_{i-n}^x}\right)\left(\sum F_{i-n}^x - A\right) \quad (3.0)$$

Here, E_i is the amount removed from the top layer (x) and added to the next layer down, $(0+1)$ of grainsize fraction i. A represents the correct thickness of the active layer $(2D90 \text{ or } 41)_{90}$. For erosion or degradation, material is moved up from the lower layers according to equation 4.

$$E_1 = \left(\frac{F_i^{x+1}}{\sum F_{i-n}^{x+1}}\right)\left(A - \sum F_{i-n}^x\right) \quad (4.0)$$

Both these expressions propagate upwards and downwards, respectively, allowing the displacement of material through the active layers. The total volume computed from this study for the accretion and as well as eroded material was 2,637,990.7 m³. The volumes computed from the dataset showed that the sediment of erosion volume is higher than the mass of material deposited from the study area, as shown in Figure 4.

3.3 Data Processing using Valeport Datalog X2 Software

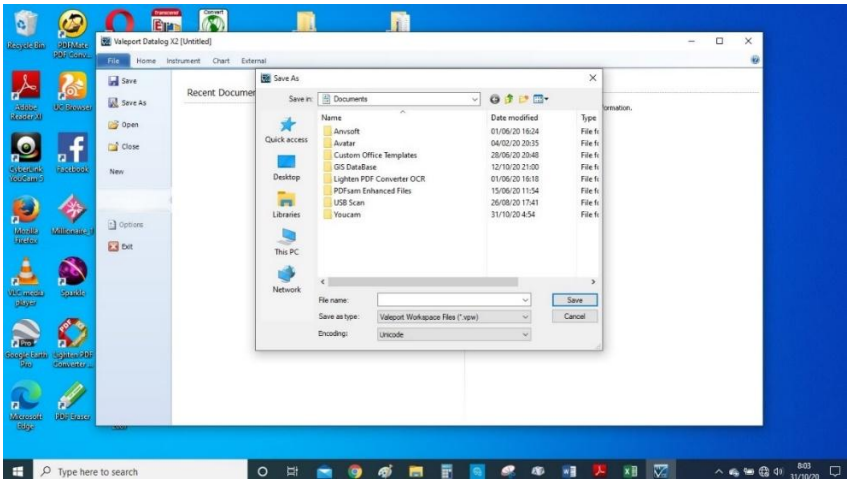

Figure 2: Datalog X2 Page Showing the 'Save As' Dialog

The Datalog X2 is one of the latest generations of software from Valeport Limited to interface, configure, and download data from Valeport instrumentation. For the Valeport CM 100 brand, the same program is sufficient for both the data logging in the field and the data processing after field work (see Figure 2). The process for data processing here is as follows:

i. On the office desk, the Datalog X2 program is opened in the PC, and the saved logged data is retrieved using 'Open' from the main tool.
ii. The opened file comes as a Valeport Workspace File with the VPW extension. At this stage, the file makes little or no sense to the reader.
iii. Using the 'Save As' tool, the file is saved as a delimited text file (TXT) in a new folder on the PC, and the Datalog X2 program is closed (as seen in Figure 2).
iv. Finally, the text file is opened using the Microsoft Excel program on the PC, and the file is converted to an Excel file with the (XLSX) extension. In Excel format, the information in the file is better expressed and understandable.

4. RESULTS

4.1 Results & Discussion

The results of this research work are expounded under this section. In assessing the positional shifts of the buried infrastructure. Sub-bottom profiles acquired in 2018 (Figure 3) revealed a fully buried pipeline with an estimated cover of 3.0 m, embedded within well-laminated, cohesive sediments, well-stratified, higher-reflectivity sediments. The layers show continuous, laminated reflectors, indicative of compacted silty-clay deposits. The burial is complete, and the pipe is not visible at the surface, implying a more stable sedimentary environment during this time. This profile suggests favorable cover and low exposure risk. In contrast, the 2024 profile (Figure 3a) shows the pipeline buried ~0.3 m (2024 Profile). The sub-bottom profile reveals a relatively shallow burial depth of approximately 0.3 m, indicating partial exposure of the pipeline. The upper layer exhibits low acoustic impedance, suggesting it is composed of soft, unconsolidated sediments. Likely, the overlying sediment mound appears discontinuous, and the acoustic shadow beneath the pipeline confirms the presence of a dense object (the pipeline), indicating a significant loss of sediment cover, with only 0.3 m of soft overburden remaining. This reflects potential sediment instability or active bedform migration, exposing the pipeline to hydrodynamic forces and increasing the risk of mechanical damage or free-spanning. The movement of sediment particles is influenced by various forces, including hydrodynamic forces generated by water flow. When sediment is unstable or bedforms are actively migrating, as mentioned in the statement, it indicates a dynamic environment where sediment

particles are in motion due to the action of water currents. The presence of sediment instability or active bedform migration suggests that the sediment bed is in a state of flux, with particles being eroded, transported, and deposited in different locations. This can expose pipelines or other submerged structures to increased hydrodynamic forces, such as drag and lift forces exerted by moving water. The risk of mechanical damage or free-spanning (where the pipeline is not supported by the seabed) is also heightened in such environments, as the movement of sediment can interact with the pipeline, potentially causing it to become dislodged, bent, or damaged. Overall, the statement aligns with the theory of sediment transport by highlighting the influence of sediment dynamics and hydrodynamic forces on the stability and integrity of submerged structures in aquatic environments. The movement of sediment particles and its implications on submerged structures in aquatic environments have been well documented in the literature. Cole *et al*. (1990) discussed the role of bedforms in sediment dynamics and their impact on pipeline stability. Similarly, Nielsen and Hansen (1999) studied the effects of sediment mobility on the design and maintenance of offshore structures. Fubara *et al* (2020), emphasize the importance of considering sediment dynamics and hydrodynamic forces when assessing the integrity of pipelines and other submerged structures in dynamic environments.

Also, this shallow cover indicates a potential scour or sediment erosion zone, increasing exposure risk. Table 3 shows the positional shift of the sub-bottom infrastructure, indicating 2-3m southward lateral displacement between the compared epochs. In assessing the seabed morphodynamics of the section of the New Calabar River, Figure 4 shows the graph that illustrates a dynamic seabed morphology, where the red color of the central section indicates the volume of erosion, while the blue color of the upstream and downstream ends indicates the volume of sediment deposition (accretion). It shows a comparative seabed profile along a surveyed section of the New Calabar River for the years 2018 (red) and 2024 (blue). Accretion zones are observed where the 2024 seabed profile lies above the 2018 profile, indicating sediment deposition. Conversely, erosion zones are evident where the 2024 profile dips below that of 2018, reflecting sediment loss. The central region from 0.7km to 1.6 km shows significant erosion, posing a potential risk to subsea infrastructure due to reduced sediment cover. In contrast, zones near the profile start and end indicate accretion, suggesting localized sediment accumulation and possibly improved burial conditions for pipelines. Table 5 shows the flow velocity measurement result in m/s, and it presents daily average flow velocity data recorded at three monitoring points, CM1, CM2, and CM3, and Figure 5 presents the chart highlights temporal variations in river flow velocity across three points.

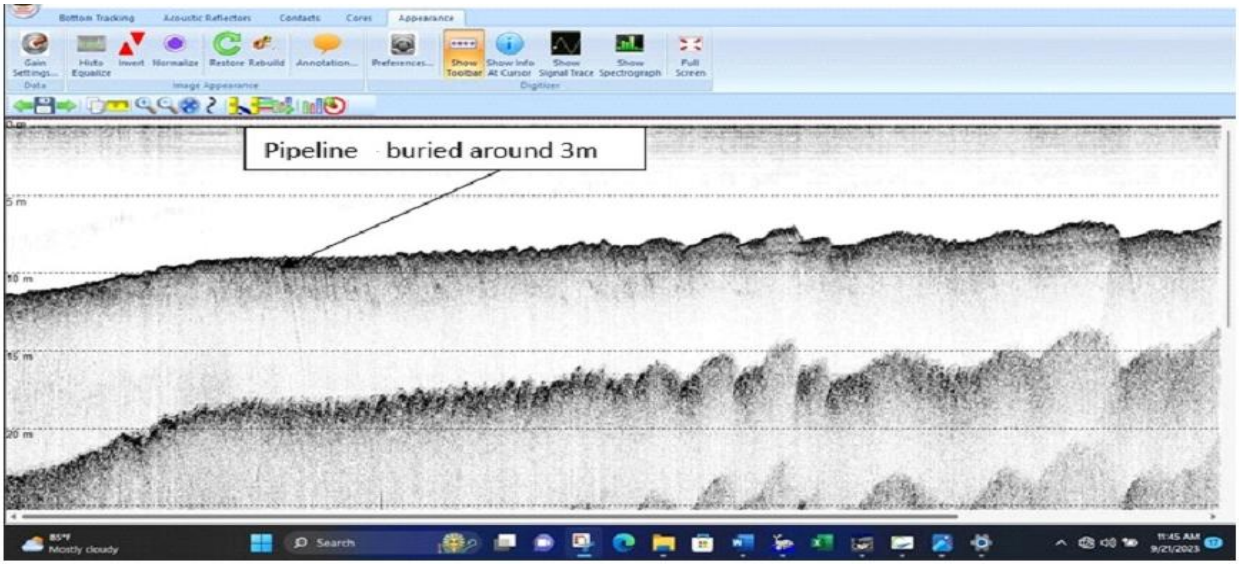

Figure 3: Subsea Profile Graph of 2018 showing fully buried Pipeline.

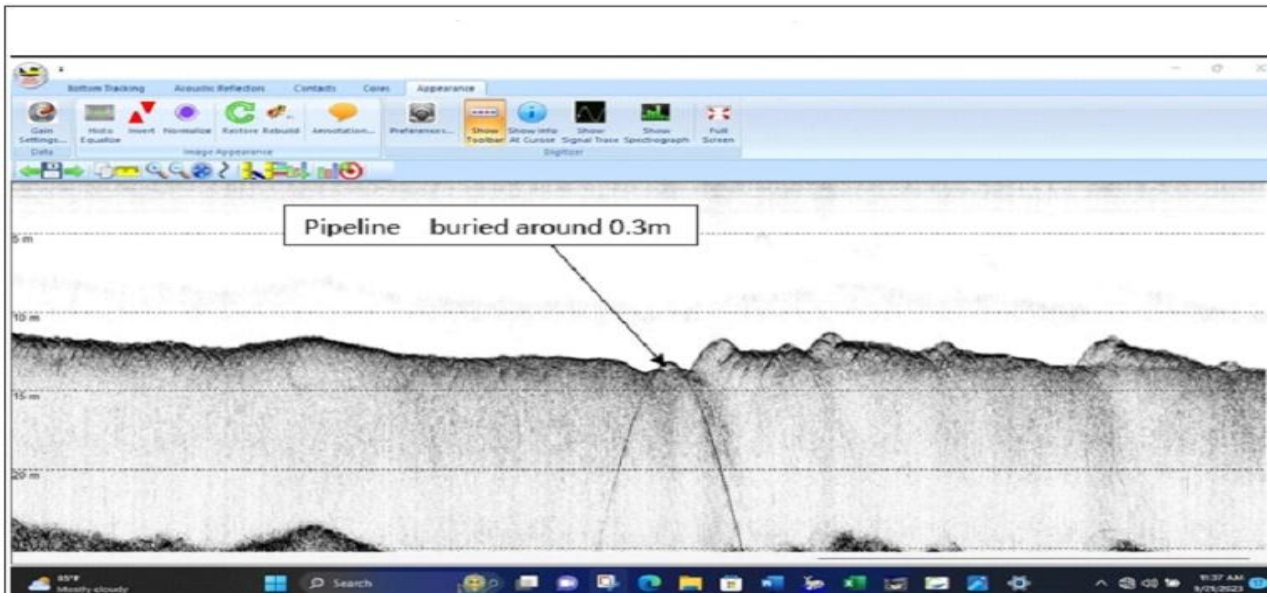

Figure 3a: Subsea Profile Graph of 2024 Showing Partial Exposure of Pipeline

Table 2: Sub-bottom Profiling Specimen Data of Post and Check with their Differences 2018/2024

S/N	Easting	Northing	Depth 2018	Depth 2024	Depth diff (2018/2024)
1.	277712.7	506262.3	3.01	3.5	0.50
2.	277659.1	506258.8	2.995	3.3	0.305
3.	277609.2	506255.6	3.018	3.5	0.482
4.	277559.3	506252.1	3.013	3.6	0.587
5.	277509.4	506249.2	2.998	3.7	0.702
6.	277459.5	506245.9	3.0	2.9	-0.10
7.	277409.6	506242.5	2.981	2.6	-0.381
8.	277359.7	506239.5	2.99	1.8	-1.19
9.	277309.8	506236.3	2.894	1.1	-1.794
10.	277259.9	506232.9	2.886	1.3	-1.586
11.	277210.1	506229.8	2.897	1.2	-1.697
12.	277160.1	506226.5	2.986	1	-1.986
13.	277110.2	506223.4	2.994	1.3	-1.694
14.	277060.3	506220.2	2.876	1.25	-1.626
15.	277010.4	506216.9	2.875	1.1	-1.775
16.	276960.5	506213.7	2.909	0.81	-2.099
17.	276910.6	506210.6	2.951	1.3	-1.651
18.	276860.7	506207.3	2.991	0.42	-1.691
19.	276800.7	506200.1	2.899	0.31	-2.589
20.	276760.9	506200.9	2.997	1.5	-1.497
21.	275912.6	506144.2	2.98	3.15	0.17
22.	275862.7	506140.7	2.992	3.01	0.018
23.	275812.8	506137.3	3.00	3.4	0.4
24.	275762.9	506133.9	3.00	3.5	0.5
25.	275713	506130.3	3.005	3.6	0.595
26.	275663.1	506126.8	3.01	3.6	0.59
27.	276411.6	506178.6	2.966	1.3	-1.666

Table 3: Specimen of the Positional Shift of Subsea Infrastructure from 2018 to 2024

PTID	EASTING	NORTHING (2018)	EASTING	NORTHING (2024)	DIST(m)	DEGREE OF SHIFT
PT1	276012.43	506320.734	276012.48	506319.96	0.77	0° 0′ 0.025″
PT2	276062.31	506323.908	276062.47	506321.41	2.51	0° 0′ 0.081″
PT3	276112.21	506327.083	276112.6	506324.6	2.51	0° 0′ 0.081″
PT4	276162.13	506330.259	276161.85	506327.74	2.54	0° 0′ 0.082″
PT5	276212.08	506333.434	276212.06	506330.93	2.5	0° 0′ 0.081″
PT6	276261.93	506336.608	276262.22	506334.12	2.51	0° 0′ 0.081″
PT7	276311.83	506339.783	276312.01	506337.29	2.5	0° 0′ 0.081″
PT8	276361.71	506343.23	276361.45	506340.44	2.6	0° 0′ 0.084″
PT9	276411.61	506346.132	276411.5	506343.62	2.51	0° 0′ 0.081″
PT10	276461.51	506349.307	276461.44	506346.8	2.51	0° 0′ 0.081″
PT11	276511.41	506352.481	276512.13	506350.02	2.56	0° 0′ 0.083″
PT12	276561.31	506355.889	276561.22	506353.15	2.74	0° 0′ 0.089″
PT13	276611.13	506360.329	276611.33	506356.33	2.54	0° 0′ 0.082″
PT14	276661.11	506362.219	276661.1	506359.5	2.72	0° 0′ 0.088″
PT15	276711.02	506365.181	276711.17	506362.69	2.49	0° 0′ 0.081″
PT16	276761.03	506368.355	276760.89	506365.85	2.52	0° 0′ 0.081″
PT17	276810.91	506371.531	276810.92	506369.03	2.5	0° 0′ 0.081″
PT18	276860.71	506374.705	276860.63	506372.2	2.51	0° 0′ 0.081″
PT19	276910.62	506377.881	276910.91	506375.39	2.51	0° 0′ 0.081″
PT20	276960.51	506381.056	276961.08	506379.34	2.4	0° 0′ 0.078″
PT21	277010.42	506384.109	277010.4	506381.72	2.39	0° 0′ 0.077″
PT22	277060.31	506387.405	277060.08	506384.89	2.53	0° 0′ 0.082″
PT23	277110.2	506390.701	277110.18	506388.07	2.63	0° 0′ 0.085″
PT24	277160.11	506393.755	277160.29	506391.26	2.51	0° 0′ 0.081″
PT25	277210	506397.031	277210.18	506394.01	3.03	0° 0′ 0.098″

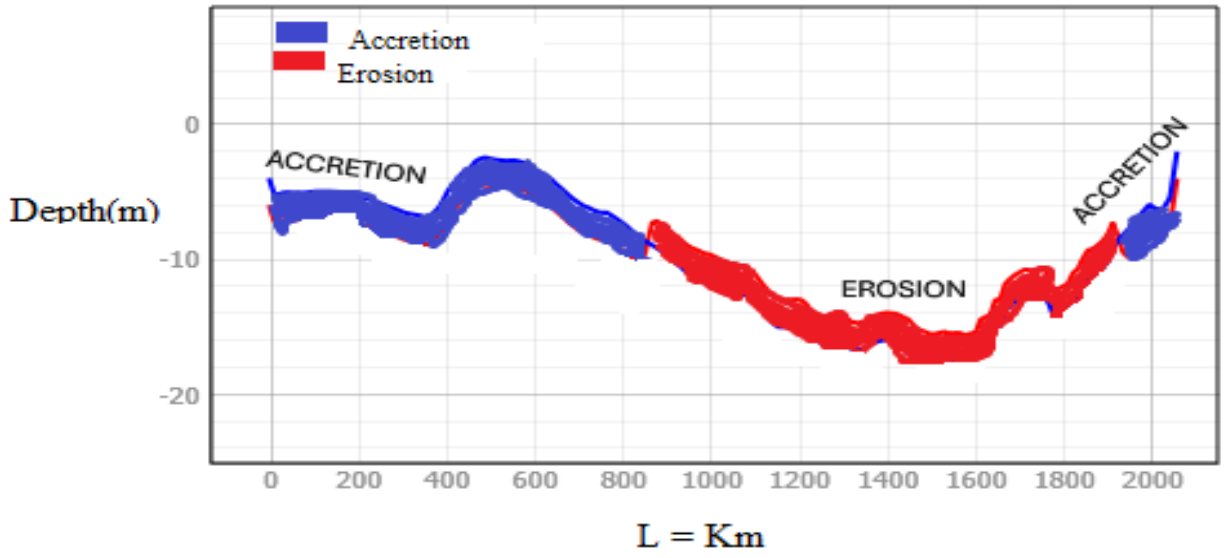

Figure 4: Profile Graph showing the Volume of Accretion and Erosion

Table 5: Flow Velocity Measurement Results in m/s Valeport 106 CM

Valeport 106CM	Point 1(CM1)	Point 2(CM2)	Point 3(CM)
Positions	287635.35mE 518145.09mN	287921.51mE 518397.04mN	288236.44mE 518690.31mN
9/4/2024 Daily average	0.539	0.684	0.621
9/5/2024 Daily average	0.501	0.798	0.593
9/6/2024	0.458	0.614	0.504
9/7/2024	0.496	0.553	0.430
9/8/2024	0.511	0.603	0.495
9/9/2024	0.431	0.501	0.437
9/10/2024	0.481	0.512	0.471
Weekly Average	0.488	0.604	0.508
All Average	0.532		

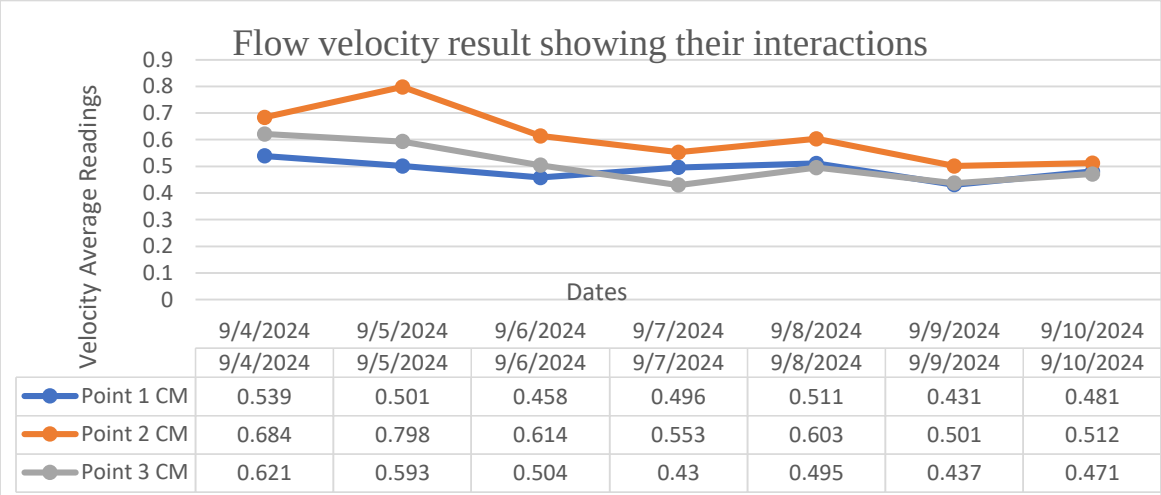

Figure 5: Flow Velocity Result Chart showing the Interaction between the daily values source

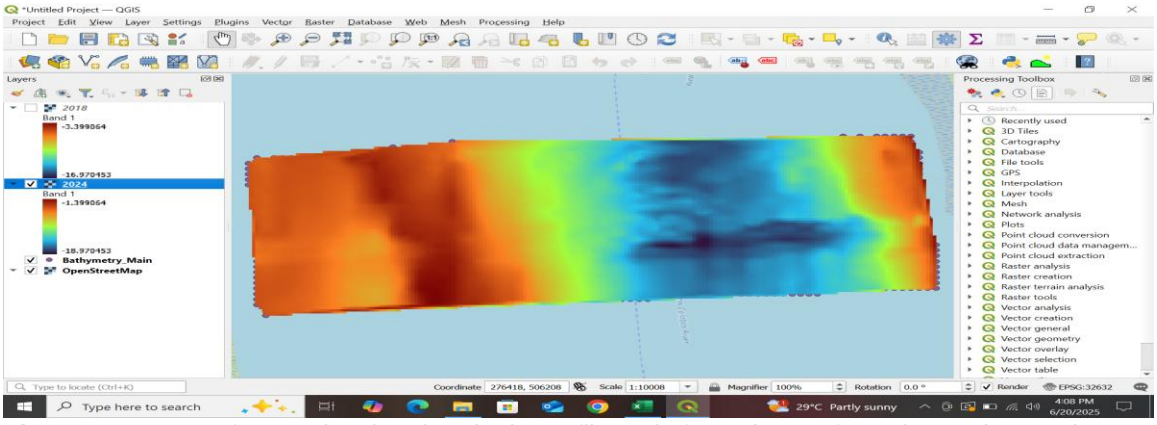

Figure 6: QGIS Software showing the plugin profile tools for Volume of Erosion and Accretion

4.1 Volumes Computation Analysis

Volume computation using a model involves a structured mathematical approach to determine how much material exists between surfaces or boundaries. The accuracy depends on the quality of the model, so this study examined the surface differencing model, which was used to compare the two surfaces spatially

referenced depth-point measurements obtained from hydroacoustic surveys to determine the deposition and erosion. The total volume computed in this study for accretion and dredged material was 2,637,990.7 m^3. The volumes computed from the dataset showed that the sediment of erosion volume is higher than the mass of material deposited in the study area.

Figure 4 satisfied the objective of determining the volume of accretion and erosion of the study area. The profile graph showed that erosion in red and accretion in blue occur when comparing the 2018 and 2024 seabed profiles. The red zones are where material has been lost, and the blue zones are where material has built up. The total volume computed from this study for the accretion was 1,010,959.09 m^3 of material that has been deposited between 2018 and 2024. It's the volume where the seabed has risen above the 2018 surface. The total volume computed for erosion was 1,627,031.61 m^3. material that has been removed between 2018 and 2024. It's the volume above the reference (2018 surface) that is now missing in the newer bathymetry survey. The volumes computed from the study area showed that eroded sediment volume is higher than the mass of the material deposited over the surveyed area, with a net volume of 616,072.52m^3. In the study area, erosion is strongly associated with shallow depths, where tidal currents are most experienced, while accretion is dominant in deeper sections, where reduced flow energy promotes sediment deposition. This explains the observed imbalance between scour and cover along the pipeline corridor.

Similarly, Figure 5 and Table 5 provided insight into the flow velocity rate of the study area. The flow velocity measurement in Table 5 showed the result of the flow measurements carried out at three different locations across the New Calabar River channel at different depths, indicating that the flow velocities are different from one point of the river to another. The flow velocity chart shows that the center of the river (CM2) recorded the highest average velocity of 0.604 m/s, while CM1 and CM3 along the banks had lower values. This gradient highlights the stronger hydrodynamic activity in the central channel, which enhances erosion and sediment transport. The results showed that elevated central velocities up to 0.798 m/s intensified sediment transport, leading to seabed changes, burial depth reduction, and a 2–3 m displacement of the pipeline.

5. DISCUSSION

The findings showed that the observed burial-depth fluctuations (3.00 → 0.30 m) and pipeline displacement (2–3 m) echo the mechanisms described by Leckie *et al*. (2018) and Cheng *et al*. (2014), who show that tidal currents and channel migration produce rapid changes in scour and cover that compromise burial depth and cause free-spanning. The larger erosion volume compared with accretion (net loss 616,072.52 m^3) reinforces documented asymmetries in sediment budgets in tidal estuaries (Ibe & Awosika, 1991; Ajdehak *et al*., 2018). Similarly, the findings show that erosion dominates in shallow, high-energy zones while accretion occurs in deeper, lower-energy sections is consistent with standard hydro-sedimentary theory and with studies that link flow energy gradients to depositional patterns (Zhang et al., 2023). The central-channel velocity peak (CM2) and higher transport capacity are the expected drivers of channel-centred incision reported in estuarine morphodynamics literature. Consequently, the flow velocity has peak velocities up to 0.798 m/s, and a mean of ~0.532 m/s is sufficient, per empirical scour relationships, to mobilize sand-sized fractions and cause net bed lowering where flows concentrate. This corroborates the causal chain reported by earlier Niger Delta studies (Eze *et al*., 2021) and recent work on vortex-induced and current-induced pipeline risks (Wu *et al*., 2025). In understanding the drivers and compounding risks, the activities of dredging, sand mining, and vessel traffic as amplifiers of natural morphodynamics align with case studies showing human activities amplify erosion, increase exposure risk, and raise the likelihood of anchor-strike events, factors emphasized in multidisciplinary assessments (Ajdehak *et al*., 2018; Leckie *et al*., 2018).

The risk prioritization of this study demonstrates that zones with reduced burial depth and high central-channel velocities should be classified as high-priority for inspection, protection (rock placement/trenching), and immediate mitigation planning. This can be further managed through engineering designs for future pipelines in similar settings should adopt dynamic burial envelopes (minimum + contingency) that account for observed net erosion rates and channel migration potential rather than static burial-depth values. The operational controls and implementation of the anchor-management and navigation restrictions within and around the identified exposure corridors will greatly reduce mechanical damage risk. This is in addition to continuous updating of burial-depth inventories, and a mandatory geospatial reporting protocol for

dredging/sand-mining would reduce surprise exposure and improve regulation. In view of the need to engage in future research, we require an increase in the temporal resolution of bathymetric surveys. We can progress from multi-year to annual or semi-annual multibeam surveys in high-risk corridors to capture seasonal variability and episodic events. Also, deploy ADCP/velocity profilers and bottom-mounted sensors (pressure sensors, seabed tiltmeters) to capture temporal variability of flows and near-bed shear stress that drive scour. Furthermore, install permanent GNSS-controlled seabed markers (or geodetic monuments) for precise horizontal/vertical displacement monitoring of pipelines.

6. CONCLUSION

The study investigated subsea infrastructure changes along a section of the New Calabar River by comparing bathymetric and sub-bottom profiler datasets acquired in 2018 and 2024. The results revealed significant alterations in seabed morphology, including both erosion and accretion zones, which directly affected burial depths and pipeline stability. The comparison of seabed configurations between 2018 and 2024 revealed significant morphological changes, including both sediment accretion and scouring or erosion. Minimum depths changed from 3.37 m to 1.36 m, and maximum depths increased from 17.204 m to 19.06 m, with the geospatial locations indicating active sediment transport processes within the study area, while volumetric computations showed approximately 1,627,031.61 m^3 of erosion and 1,010,959.09 m^3 of accretion across the study corridor.

Positional assessment further demonstrated a southward shift of 2–3 m in subsea pipelines. The finding is consistent with international studies that have documented meter-scale lateral movements of pipelines under similar hydrodynamic and sediment transport conditions. For instance, DNV-RP-F109 establishes that pipelines in mobile seabed environments can undergo meter-scale displacements due to current and wave action (DNV, 2015). Likewise, the PHMSA river-scour monitoring program and the Yellowstone River risk assessment reported that riverbed scour and channel migration can laterally shift buried pipelines by several meters, exposing them to structural risks (PHMSA, 2019; Upper Great Plains Transportation Institute, 2014). Furthermore, guidance from the ASME International Pipeline Conference highlights that lateral channel migration can displace pipelines by 2–5 m, aligning closely with the displacement observed in this study (ASME, 2016). Beyond fluvial effects, Carr, Mokhtari, and Palmer (2018) also demonstrated that pipeline walking and lateral buckling mechanisms can result in cumulative lateral displacements of similar magnitude.

Hydraulic modeling using Manning's equation confirmed that flow velocities in parts of the river exceeded thresholds for sediment mobility, predisposing shallow buried pipelines to scour and exposure. Sediment analysis revealed that coarse-grained deposits contributed to relative stability, while finer sediments were more vulnerable to erosion and displacement. Collectively, these findings highlight the dynamic and unstable nature of the New Calabar River channel, with direct implications for subsea infrastructure safety, asset integrity, and environmental risk management.

The study underscores that continuous monitoring, volumetric change assessment, and positional shift analysis are indispensable for protecting oil and gas pipelines in dynamic river systems. Such proactive measures not only strengthen infrastructure resilience but also mitigate risks of environmental contamination and disruptions to energy supply. By integrating geospatial monitoring with risk management, the findings directly contribute to SDG 7 (Affordable and Clean Energy) through the protection of critical energy infrastructure, ensuring reliable and sustainable energy delivery. Furthermore, minimizing pipeline exposure and potential leakages supports SDG 14 (Life Below Water) by safeguarding aquatic ecosystems from hydrocarbon pollution, and SDG 15 (Life on Land) by preventing soil and habitat degradation in surrounding terrestrial environments. These outcomes reinforce both local observations and global evidence on subsea infrastructure vulnerability in morphologically unstable waterways (DNV, 2015; PHMSA, 2019; Upper Great Plains Transportation Institute, 2014; ASME, 2016; Carr *et al*., 2018).

6.1 Recommendation

Based on the findings of this study, the following recommendations are proposed:

1. Continuous Monitoring**:** This study has been able to obtain exact positional information regarding the subsea infrastructure. It is recommended that regular bathymetric and sub-bottom surveys be conducted to track seabed changes, burial depth variations, and positional shifts of subsea infrastructure.
2. Pipeline Protection Measures**:** This research has been able to carry out a comprehensive study on a section of the New Calabar River. The result showed that sections of pipeline found to be at risk of exposure due to erosion should be reinforced through protective measures, such as trenching, rock dumping, or the use of engineered coverings.
3. Hydrodynamic Modeling: Detailed numerical modeling of flow velocities and sediment transport should be undertaken to predict future scour and accretion patterns, supporting proactive decision-making.
4. Regulatory Oversight: This research work is a useful tool for agencies such as NIWA, NUPRC, and NIMASA; they should strengthen regulatory frameworks to ensure operators comply with minimum burial depths, anchorage restrictions, and periodic inspection requirements.
5. Operational Awareness: Navigation and anchorage policies along the New Calabar River should be reviewed to minimize anchor-dragging risks near subsea infrastructure corridors.

REFERENCES

Ajdehak, E., Zhao, M., & Cheng, S. (2018). Numerical investigation of local scour beneath a sagging subsea pipeline in steady currents. *Coastal Engineering, 136*, 106–118.

Basil, D. D. (2024). Assessment of the accuracies of multibeam calibration values and the depth between real-time kinematics and precise point positioning. *Journal of Geomatics and Environmental Research, 7*(1).

Carroll, J., & Harris, P. (2002). Biological colonization of offshore structures: Influence of burial depth and sediment type. *Marine Environmental Research, 54*(3), 201–215.

Carr, D., Bradman, T., & Suter, P. (2018). The effects of climate change on bird populations. *Conservation Biology, 32*(6), 1351–1360.

Carr, M., Mokhtari, S., & Palmer, A. (2018). Pipeline walking and lateral buckling: Mechanisms and mitigation. *Proceedings of the Offshore Technology Conference*, Houston, Texas.

Cheng, Y.-H., Ho, C.-R., Zheng, Q., & Kuo, N.-J. (2014). Statistical characteristics of mesoscale eddies in the North Pacific derived from satellite altimetry. *Remote Sensing, 6*(6), 5164–5183. https://doi.org/10.3390/rs6065164

Chiew, Y. M. (1993). Local scour around a submarine pipeline with a spoiler attachment. In *Proceedings of the 3rd International Offshore and Polar Engineering Conference*, Singapore.

Cole, S., Shroder, J. F., Huestis, S., et al. (1990). Bedforms and flow regime architecture in an environment of rapid sedimentation, Mina Al-Ahmadi Lagoon, Kuwait. *Journal of Sedimentary Petrology, 60*(6), 832–846.

Det Norske Veritas. (2015). *Recommended practice: On-bottom stability of submarine pipelines (DNV-RP-F109)*.

Eke, J. C., Huuse, M., & Sofoluwe, P. (2021). Sediment dynamics and infrastructure stability in Nigerian inland waterways. *Journal of Coastal Research, 37*(4), 678–690.

Eze, P. I., Kurotamuno, P. J., & Kpama, S. B. (2022). Assessment of bathymetric components of the Ogbogoro section of New Calabar River, Rivers State, Nigeria. *International Journal of Research Publication and Reviews, 3*(7), 309–320.

Fubara, D. M. J., Hart, L., & Otansanya, G. I. (2020). Navigational hazard analysis of part of Bonny River, Rivers State, Nigeria. *Journal of Geosciences and Geomatics, 8*(1), 25–34. https://doi.org/10.12691/jgg-8-1-4

Ibe, A. C., & Awosika, L. F. (1991). Sea-level rise impact on African coastal zones. In S. H. Omide & C. Juma (Eds.), *A change in weather: African perspectives on climate change* (pp. 105–112). African Centre for Technology Studies.

Leckie, S. H. F., Draper, S., White, D. J., Cheng, L., Griffiths, T., & Fogliani, A. (2018). Observed changes to the stability of a subsea pipeline caused by seabed mobility. *Ocean Engineering, 169*, 159–176.

Nielsen, P., & Hansen, E. (1999). Coastal erosion and accretion. In C. R. Thorne, J. D. Hey, & M. D. Newson (Eds.), *Applied Coastal Geomorphology* (pp. 241–264). John Wiley & Sons.

Olobayo, T., Huuse, M., & Sofoluwe, I. (2024). Geo-mechanical review of submarine landslides in the Niger Delta margin. *Environmental Earth Sciences*.

Orupabo, S. (2002). Evaluating beach sediment failure states along Nigerian coastline. *Journal of Modeling Design and Management of Engineering Systems, 1*(1).

Oye, O. M., Hart, L., & Orupabo, S. (2021). Bathymetric components towards ensuring navigable channel along a section of Lower River Niger, Lokoja, Kogi State, Nigeria. *International Journal of Hydrology, 5*(5), 231–238. https://doi.org/10.15406/ijh.2021.05.00285

PHMSA. (2019). *Pipeline river crossings: Research and development for monitoring and mitigation of river scour*. Pipeline and Hazardous Materials Safety Administration.

Udosoh, N. E., Idiapho, C. A., & Awwal, S. (2020). Material selection for subsea pipeline construction under uncertainties for the Niger Delta region. *Journal of Engineering Research and Reports*.

Upper Great Plains Transportation Institute. (2014). *(Publication details not provided)*.

Wu, W., Yang, H., & Sun, W. (2025). Analysis of disturbance and safety risks to shallow-buried pipelines from tunneling activities. *Buildings, 15*(13), 2253. https://doi.org/10.3390/buildings15132253

Yang, L. P., Shi, B., Guo, Y. K., Zhang, L. X., Zhang, J. S., & Han, Y. (2014). Scour protection of submarine pipelines using rubber plates underneath the pipes. *Ocean Engineering, 84*, 176–182.

Zhang, Z., Chiew, Y., & Ji, C. (2023). Equilibrium depth and time scale of local scour around a forced vibrating pipeline. *Coastal Engineering, 185*, Article 104378.